JACS
JOURNAL OF THE AMERICAN CHEMICAL SOCIETY

Subscriber access provided by ISTANBUL TEKNIK UNIV

Communication

Nernstian Adsorbate-like Bulk Layer of Organic Radical Polymers for High-Density Charge Storage Purposes

Kenichi Oyaizu, Yuko Ando, Hiroaki Konishi, and Hiroyuki Nishide

J. Am. Chem. Soc., **2008**, 130 (44), 14459-14461 • DOI: 10.1021/ja803742b • Publication Date (Web): 09 October 2008

Downloaded from http://pubs.acs.org on February 8, 2009

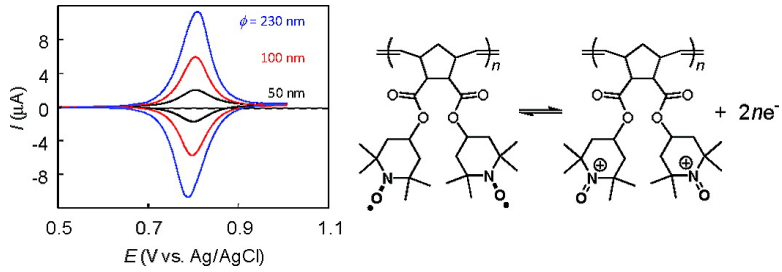

More About This Article

Additional resources and features associated with this article are available within the HTML version:

- Supporting Information
- Access to high resolution figures
- Links to articles and content related to this article
- Copyright permission to reproduce figures and/or text from this article

View the Full Text HTML

ACS Publications
High quality. High impact.

Journal of the American Chemical Society is published by the American Chemical Society. 1155 Sixteenth Street N.W., Washington, DC 20036

J|A|C|S
COMMUNICATIONS

Published on Web 10/09/2008

Nernstian Adsorbate-like Bulk Layer of Organic Radical Polymers for High-Density Charge Storage Purposes

Kenichi Oyaizu, Yuko Ando, Hiroaki Konishi, and Hiroyuki Nishide*

Department of Applied Chemistry, Waseda University, Tokyo 169-8555, Japan

Received May 19, 2008; E-mail: nishide@waseda.jp

Electrical conduction by concentration gradient driven charge transport throughout nonconjugated redox polymer layers offer possibilities of using them as organic conducting materials in various wet-type devices for energy conversion and storage, such as dye-sensitized solar cells and secondary batteries.[1] Here we report that even tens to hundreds nanometer thick redox polymer layers functionalized with 2,2,6,6-tetramethylpiperidin-1-oxyl-4-yl (TEMPO) groups show nernstian adsorbate-like behaviors, based on a fast charge propagation within the bulk layer and persistency in electrolyte solutions. Such capability was pursued also with a view to maximize a storage capacity of organic batteries,[2] using organic polymers as electrode-active materials.[3]

Electron transport initiated by applying an electrode potential to a redox polymer layer bathed in electrolyte solutions amounts to the propagation of charge through the layer until all of the redox sites change their oxidation state. When the sites are immobilized in the layer allowing only diffusional collision of the neighboring sites to undergo an electron self-exchange reaction, this process involves an electron hopping mechanism with a diffusion coefficient given by $D = k_{ex}\delta^2 C^*/6$, where k_{ex} is the bimolecular rate constant, δ the site distance, and C^* the site concentration in the layer.[4] One could approximate that all redox sites in the layer, even not immediately adjacent to the electrode surface, would be almost equilibrated with the electrode potential when it is scanned sufficiently slowly to accomplish $(Dt)^{1/2} > \phi'$, where ϕ' is the swollen layer thickness. The result is a nernstian monolayer-like reaction, giving rise to a cyclic voltammogram with equal anodic and cathodic peak potentials ($E_{pa} = E_{pc}$) and a peak current density given by $i_p = n^2F^2v\Gamma^*/(4RT)$ where v and Γ^* are the scan rate and the total electroactive coverage, respectively.[5] However, there have been few reports of its occurrence with conventional redox polymers.[6] Layers of poly(vinylferrocene) typically display cyclic voltammograms with nonideal shapes, which have been attributed to site interactions[7] and oxidation state-dependent layer resistance to counterion transport.[8] Elution of polymers during potential cycling also results in dissimilar anodic and cathodic waves. We anticipate that the ideal behavior, free from those limitations, is advantageous for use as electrode-active materials in rechargeable batteries, since it would maximize the redox capacity of the polymer loaded on a current collector and minimize the internal resistance to improve the rate performance. In this report, we focus on redox polymers with TEMPO functionality,[9] prompted by recent findings of the fast electrode kinetics of a monomeric TEMPO/TEMPO$^+$ couple with a heterogeneous rate constant of $k_0 = 8.4 \times 10^{-1}$ cm s^{-1} and a rapid electron self-exchange with $k_{ex} \approx 10^8$ M^{-1} s^{-1} in solutions.[10]

A cross-linkable polynorbornene **1** ($M_n = 3.3 \times 10^4$, $M_w/M_n = 1.1$) densely populated with the pendant TEMPO groups was designed by incorporating a small amount of coumarin units (Scheme 1). The coumarin content in **1** was controlled by the feed ratio of the two monomers for the ring-opening metathesis copolymerization (Table S1).

Scheme 1. Synthesis of the TEMPO-Substituted Polynorbornene Containing the Coumarin Unit (**1**)

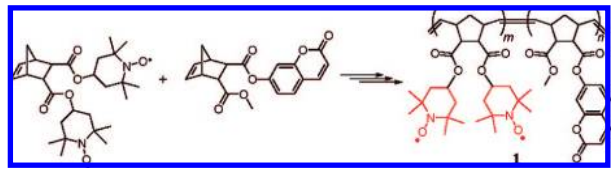

A large population of the TEMPO pendants in **1** produced a broad featureless ESR spectrum even in dilute solution, as a result of a locally high density of unpaired electrons. A CH_2Cl_2 solution of **1** showed a unimodal ESR signal at $g = 2.0072$ due to the spin exchange interaction between the unpaired electrons of the neighboring TEMPO group (Figure 1b), in contrast to the spectrum obtained for a solution of the TEMPO-substituted norbornene monomer which revealed a hyperfine structure resulting from the nitrogen-centered ($I = 1$) radical (Figure 1a). These spectra persisted without change for weeks at room temperature under air, which demonstrated the durability of the nitroxide radicals.

Electrode reaction of **1** in electrolyte solutions yielded a single voltammetric wave due to the TEMPO/TEMPO$^+$ couple with a magnitude of the current determined by the number of TEMPO groups present. The multiple, noninteracting redox behavior was based on the presence of many unpaired electrons each localized on different TEMPO groups, which gave rise to a paramagnetic response in a magnetization experiment. Static magnetic susceptibility of **1** was determined by SQUID measurements at 0.5 T and

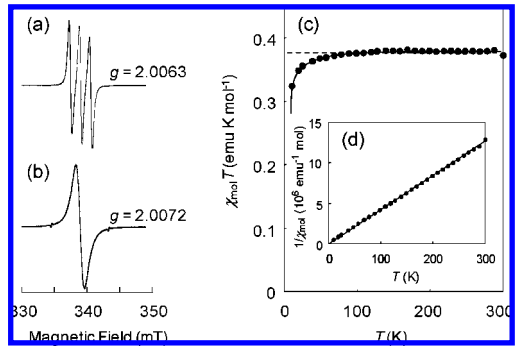

Figure 1. ESR spectra obtained for the solutions of the monomer, norbornene-2,3-dicarboxylic acid bis(2,2,6,6-tetramethylpiperidin-1-oxyl-4-yl) ester (0.1 mmol L^{-1}), (a) and **1** ($m/n = 0.85/0.15$, 0.1 mmol unit L^{-1}) (b) in CH_2Cl_2 at room temperature; $\chi_{mol}T$ versus T (c) and $1/\chi_{mol}$ versus T plots with the Curie−Weiss fitting (solid line) (d) for **1** (19.9 mg) obtained by SQUID measurements, where χ_{mol} is based on per mol of the nitroxide radical. Small signals near 334 and 343 mT in panel b are from the Mn^{2+}/MgO standard. Dotted line in panel c represents the theoretical value of $\chi_{mol}T$ for $S = {}^1/_2$.

 © 2008 American Chemical Society

Scheme 2. Structure of the Photo-crosslinked Polymer (**2**) Containing the Dimerized Coumarin Bridge

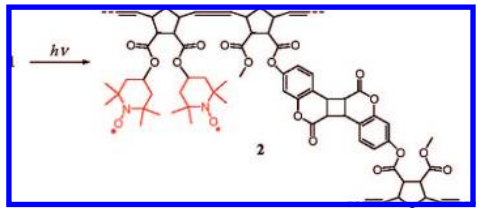

at various temperatures from 1.95 to 270 K. The resulting $\chi_{mol}T$ values at high temperatures corresponded to 0.375 emu K mol^{-1} calculated for a spin quantum number of $S = {}^1/_2$, which supported the paramagnetic property (Figure 1c). The deviation of $\chi_{mol}T$ to lower values at low temperatures indicated a weak through-space antiferromagnetic interaction within the polymer.

The unpaired electron density in **1** was determined from the $1/\chi_{mol}$ versus T plots (Figure 1d), based on the Curie−Weiss rule according to $1/\chi_{para} = T/C - \theta/C$ where C is a Curie constant defined as $N_e g^2 \mu_B{}^2 S(S + 1)/(3k_B)$. The slope of the $1/\chi_{mol}$ versus T plots corresponded to $1/C$ and gave an unpaired electron density of $N_e = 1.95 \times 10^{21}$ spin/g for **1** with a composition of $m/n = 0.85/0.15$, which corresponded to 85% of the existing TEMPO units in the polymer. The paramagnetic nature of **1** at room temperature also allowed determination of the unpaired electron density of ~90% by simply integrating the ESR signal with a TEMPO standard, which roughly agreed with that from the SQUID measurement.

The coumarin unit in **1** underwent cycloaddition by UV irradiation to form bridges (Scheme 2).[11] The photo cross-linking was accomplished by irradiation of 8.1 J/cm^2 UV light using a low-pressure Hg lamp at a thin layer of **1** prepared on a quartz glass substrate. The progress of the cross-linking was monitored by UV−vis spectroscopy using the absorption band of coumarin at $\lambda_{max} = 320$ nm. The band gradually decreased in intensity during the course of the irradiation and disappeared after 20 min, which indicated a high conversion to the coumarin dimer in **2**. SQUID measurements gave the unpaired electron density of 87% for **2** with respect to that for **1**, which revealed that many nitroxide radicals survived in **2**.

The polymer **2** is characterized by a redox capacity of 72 mAh/g based on the unpaired electron density, which is much larger than the formula weight-based theoretical capacities of the already existing redox polymers that exhibit a nernstian monolayer-like behavior, such as poly(allylamine) derivatized with Os(bpy)$_2$ClPy (39 mAh/g)[6a] and a viologen-containing polymer (51 mAh/g).[6c]

The spin-coating and photo-cross-linking strategy using an ethyl lactate solution of **1** afforded a uniform layer of **2** on an electrode surface. Contact stylus profile near a scratched edge gave a thickness ϕ under dry conditions in the range of 50−230 nm according to the concentration of **1** in the mother liquor and the spinning velocity and revealed a flat surface with a roughness of less than 4 nm.

Cyclic voltammograms obtained for the layer with a sufficient cross-linking density of 15% persisted without change for several days of continued charging/discharging cycling in CH_3CN, in which the layer appeared completely insoluble (Figure 2a). The nernstian adsorbate-like behavior of the layer at $\phi = 50$ nm ($\Gamma^* = 1.4 \times 10^{-8}$ mol cm^{-2}) was demonstrated by the negligible peak-to-peak separation ($\Delta E_p = 5$ mV) and the peak current which was consistent with Γ^* and proportional to v in the range of 1−5 mV s^{-1} (Supporting Information, Figure S1). Wave shapes with slightly larger ΔE_p (8 and 22 mV at $\phi = 100$ and 230 nm, respectively) suggested some contribution from diffusion across the thicker layers.

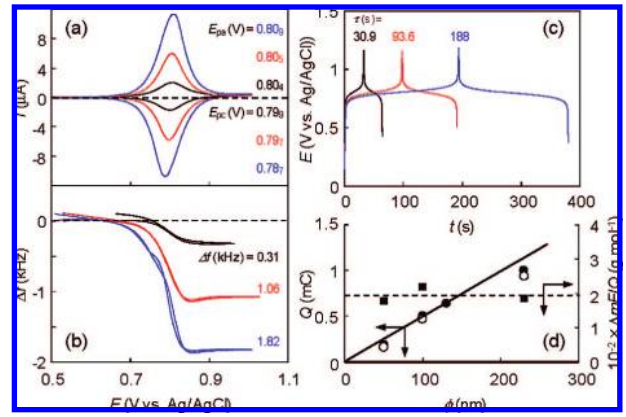

Figure 2. (a) Cyclic voltammograms for the layers of **2** ($m/n = 0.85/0.15$) with $\phi = 50$ (black curve), 100 (red), and 230 nm (blue) at a scan rate of 1 mV s^{-1}. The electrolyte was a solution of 0.1 M tetrabutylammonium perchlorate in CH_3CN. The polymer layer was prepared on a gold disk with an area of $A = 0.196$ cm^2 at the surface of a QCM assembly (see Supporting Information). (b) Frequency curves obtained simultaneously with panel a. (c) Chronopotentiograms for the oxidation followed by the reduction of the layer at $I = 0.005$ mA. (d) Plots of Q and $\Delta mF/Q$ versus ϕ, where Q and Δm were redox capacity and mass change, respectively. Q was determined from the area under the waves in panel a (○) and by $I \times \tau$ (●) where τ was the transition times in panel c. Resonant frequency changes Δf in panel b were converted to Δm by the Sauerbrey equation $\Delta f = -C_f \Delta m$ where the sensitive factor C_f was 0.183 Hz cm^2/ng. Solid line represents the formula weight-based calculated capacity according to $FA\Gamma^*$ (eq S2). Dotted line corresponds to the average of $\Delta mF/Q$ (■).

Characteristics of the adsorbate-like layer resulted in nonhysteretic QCM responses (Figure 2b). The resonant frequency decreased during the oxidation and attained its original value after the reduction, indicating reversibility to the mass change. The galvanostatic $E-t$ curves showed a plateau region (Figure 2c), which agreed with the formal potential of 0.80 V. The amount of charge consumed during the potential scan and the constant-current electrolysis both coincided with the formula weight-based capacity corrected with the unpaired electron density (Figure 2d), which revealed that all of the sites in the layer underwent the redox reaction.

The population and dynamics of solvent and ionic species in the layer gave insight into the nature of the processes responsible for the monolayer-like characteristics. Electroneutrality requires that the removal of each electron from the polymer layer result in the insertion of one ClO_4^- into the layer and/or the Donnan exclusion of the electrolyte cation. However, the mass change relative to the redox capacity ($\Delta mF/Q \approx 200$ g mol^{-1}) was much larger than the formula weight of the anion (Figure 2d), indicating that solvation was enhanced by the ionic osmotic force in the oxidized layer. Such solvent dynamics is likely to unpack polymer chains and reduce resistance to counterion transport.

Another curious issue is the ideal finite-diffusion behavior expressed by eqs 1 and 2 for constant-current chronopotentiometry and potential-step chronoamperometry, respectively,[4] resulting from the layer's uniformity and flat surface. It may be noted that these features have been difficult to accomplish with conventional redox polymers, including those employed in radical batteries.[12] The transition time constant $i\tau^{1/2}$ at different i and ϕ' changed according to eq 1 (Figure 3a). The diffusion coefficient in eq 1 ($D = 5.3 \times 10^{-10}$ cm^2 s^{-1}) was determined from the Cottrell plots (Figure 3b) for the semi-infinite diffusion which prevailed at the early stage of electrolysis ($t \ll \phi'^2 D^{-1}$), and was supported by independent normal pulse voltammetry (Figure S2). A relatively small degree of swelling of $q = 1.4$ (in v/v) at this cross-linking density corresponded to

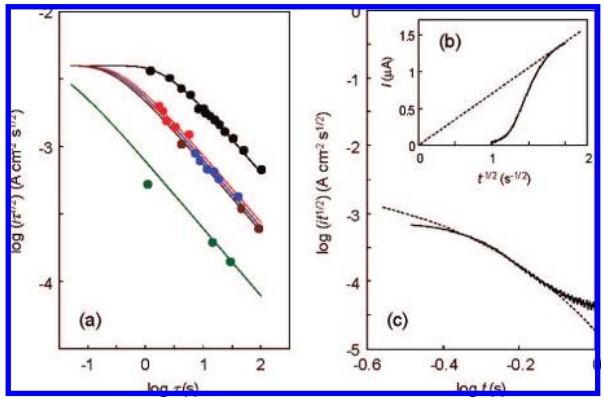

Figure 3. (a) Diffusional responses from the constant-current electrolysis of the **2** layers with different ϕ. Curves calculated from eq 1 were fitted to τ at current densities of $i = 3.3-0.067$ mA cm^{-2} in chronopotentiometry, yielding $\phi' = 330$ (black), 140 (red), 130 (blue), 120 (brown), and 40 nm (green). (b) Cottrell curve for chronoamperometry after applying a potential pulse of 0 to 1.2 V vs Ag/AgCl. The dashed line corresponds to a semi-infinite diffusion process. (c) Diffusional responses for the chronoamperometry. Solid curve was obtained experimentally in panel b. Dashed curve was calculated from eq 2 using $\phi' = 140$ nm.

$C^* = 2.0$ M in the swollen state, which was consistent with ϕ' ($= q^{1/3}\phi$) in eq 1 determined by curve fitting to the experimental plots using ϕ' as the variable parameter. The resulting constants allowed good coincidence of the transient amperogram with eq 2 (Figure 3c).

$$i\tau^{1/2} = \frac{nF(\pi D)^{1/2}C^*}{2}\left[1 + 2\sum_{m=1}^{\infty}\left\{\exp\frac{-m^2\phi'^2}{D\tau} - \frac{m\phi'\pi^{1/2}}{(D\tau)^{1/2}}\mathrm{erfc}\frac{m\phi'}{(D\tau)^{1/2}}\right\}\right]^{-1} \quad (1)$$

$$\log(it^{1/2}) = \log\left[\frac{nFD^{1/2}C^*}{\pi^{1/2}}\left\{1 + 2\sum_{m=1}^{\infty}(-1)^m\exp\frac{-m^2\phi'^2}{Dt}\right\}\right] \quad (2)$$

The electron self-exchange rate in the layer predicted from D was $k_{ex} = 1.8 \times 10^5$ M^{-1} s^{-1} using $\delta = (C^*N_A)^{-1/3}$ where N_A is the Avogadro's number. A relatively high rate of electron self-exchange in the layer reflected the outer-sphere redox reaction of the monomeric TEMPO$^{0/+}$ couple in solutions.[10c]

The diffusional behavior conformable to eqs 1 and 2 revealed that the charge propagated *throughout* the layer in a submicrometer scale. The behavior is dominated by the finite-diffusion term when the propagating front reaches the polymer/solution interface (Scheme 3). The $i\tau^{1/2}$ responses from layers with different ϕ' is thus viewed as the snapshots of the diffusing front buried in the layer, which helps to characterize the polymer as a kind of a conducting material.

Scheme 3. Charge Propagation during Oxidation of the **2** Layer Confined at the Electrode or Current Collector Surface

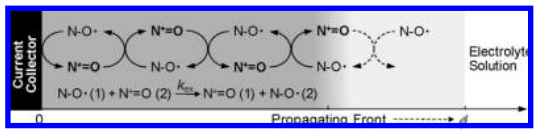

Challenges to increase D to improve transport properties for higher-rate capability of organic batteries and determination of ion permselectivity are the topics of our continuous research.

Acknowledgment. This work was partially supported by Grants-in-Aid for Scientific Research (Nos. 19105003, 19655043, 17067017, and 19022035), the Global COE program from MEXT, Japan, and the NEDO Project on "Radical Battery for Ubiquitous Power". We thank Dr. Shigeyuki Iwasa and Dr. Kentaro Nakahara of NEC Co. for technical discussion.

Supporting Information Available: Experimental details on the monomer synthesis, the polymerization and the electrode preparation, data for the degree of swelling, the plots of peak currents vs sweep rates in Figure 2a, the normal pulse voltammetric Cottrell plots, and the ^{1}H NMR spectrum of **1** after conversion to diamagnetic species by the reduction with phenylhydrazine. This material is available free of charge via the Internet at http://pubs.acs.org.

References

(1) (a) Taranekar, P.; Fulghum, T.; Patton, D.; Ponnapati, R.; Clyde, G.; Advincula, R. *J. Am. Chem. Soc.* **2007**, *129*, 12537–12548. (b) Mannes, K. M.; Terrill, R. H.; Meyer, T. J.; Murray, R. W.; Wightman, R. M. *J. Am. Chem. Soc.* **1996**, *118*, 10609–10616.
(2) (a) Nishide, H.; Oyaizu, K. *Science* **2008**, *319*, 737–738. (b) Nishide, H.; Suga, T. *Electrochem. Soc. Interface* **2005**, *14*, 32–36.
(3) (a) Oyaizu, K.; Suga, T.; Yoshimura, K.; Nishide, H. *Macromolecules* **2008**, *41*, 6646–6652. (b) Suga, T.; Konishi, H.; Nishide, H. *Chem. Commun.* **2007**, 1730–1732. (c) Suga, T.; Pu, Y.-J.; Kasatori, S.; Nishide, H. *Macromolecules* **2007**, *40*, 3167–3173. (d) Bugnon, L.; Morton, C. J. H.; Novak, P.; Vetter, J.; Nesvadba, P. *Chem. Mater.* **2007**, *19*, 2910–2914.
(4) *Molecular Design of Electrode Surfaces*; Murray, R. W., Ed.; Wiley-Interscience: New York, 1992.
(5) Bard, A. J.; Faulkner, L. R. *Electrochemical Methods, Fundamentals and Applications*, 2nd ed.; Wiley: New York, 2001.
(6) (a) Tagliazucchi, M.; Calvo, E. J.; Szleifer, I. *J. Phys. Chem. C* **2008**, *112*, 458–471. (b) Redepenning, J.; Miller, B. R.; Burnham, S. *Anal. Chem.* **1994**, *66*, 1560–1565. (c) Dalton, E. F.; Murray, R. W. *J. Phys. Chem.* **1991**, *95*, 6383–6389. (d) Shigehara, K.; Oyama, N.; Anson, F. C. *J. Am. Chem. Soc.* **1981**, *103*, 2552–2558. (e) Kelly, A. J.; Oyama, N. *J. Phys. Chem.* **1991**, *95*, 9579–9584. (f) Brown, A. P.; Anson, F. C. *Anal. Chem.* **1977**, *49*, 1589–1595.
(7) Daum, P.; Murray, R. W. *J. Phys. Chem.* **1981**, *85*, 389–396.
(8) Hillman, A. R.; Hughes, N. A.; Bruckenstein, S. *J. Electrochem. Soc.* **1992**, *139*, 74–77.
(9) (a) Yonekuta, Y.; Susuki, K.; Oyaizu, K.; Honda, K.; Nishide, H. *J. Am. Chem. Soc.* **2007**, *129*, 14128–14129. (b) Takahashi, Y.; Hayashi, N.; Oyaizu, K.; Honda, K.; Nishide, H. *Polym. J.* **2008**, *40*, 763–767. (c) Endo, T.; Takuma, K.; Takata, T.; Hirose, C. *Macromolecules* **1993**, *26*, 3227–3229.
(10) (a) Yonekuta, Y.; Oyaizu, K.; Nishide, H. *Chem. Lett.* **2007**, *36*, 866–867. (b) Suga, T.; Pu, Y.-J.; Oyaizu, K.; Nishide, H. *Bull. Chem. Soc. Jpn.* **2004**, *77*, 2203–2204. (c) Grampp, G.; Rasmussen, K. *Phys. Chem. Chem. Phys.* **2002**, *4*, 5546–5549.
(11) Lewis, F. D.; Barancyk, S. V. *J. Am. Chem. Soc.* **1989**, *111*, 8653–8661.
(12) (a) Nishide, H.; Iwasa, S.; Pu, Y.-J.; Suga, T.; Nakahara, K.; Satoh, M. *Electrochim. Acta* **2004**, *50*, 827–831. (b) Suguro, M.; Iwasa, S.; Kusachi, Y.; Morioka, Y.; Nakahara, K. *Macromol. Rapid Commun.* **2007**, *28*, 1929–1933. (c) Kim, J.-K.; Cheruvally, G.; Choi, J.-W.; Ahn, J.-H.; Choi, D. S.; Song, C. E. *J. Electrochem. Soc.* **2007**, *154*, A839−A843. (d) Zhang, X.; Li, H.; Li, L.; Lu, G.; Zhang, S.; Gu, L.; Xia, Y.; Huang, X. *Polymer* **2008**, *49*, 3393–3398. (e) Nakahara, K.; Iwasa, S.; Iriyama, J.; Morioka, Y.; Suguro, M.; Satoh, M.; Cairns, E. J. *Electrochim. Acta* **2006**, *52*, 921–927. (f) Nakahara, K.; Iriyama, J.; Iwasa, S.; Suguro, M.; Satoh, M.; Cairns, E. J. *J. Power Sources* **2007**, *163*, 1110–1113. (g) Nakahara, K.; Iwasa, S.; Satoh, M.; Morioka, Y.; Iriyama, J.; Suguro, M.; Hasegawa, E. *Chem. Phys. Lett.* **2002**, *359*, 351–354. (h) Nakahara, K.; Iriyama, J.; Iwasa, S.; Suguro, M.; Satoh, M.; Cairns, E. J. *J. Power Sources* **2007**, *165*, 398–402. (i) Nakahara, K.; Iriyama, J.; Iwasa, S.; Suguro, M.; Satoh, M.; Cairns, E. J. *J. Power Sources* **2007**, *165*, 870–873.

JA803742B